# Diagnostics of microwave plasmas at atmospheric pressure applied to the growth of organosilicon nanopowders

L. Stafford*, R.K. Gangwar, and A. Durocher-Jean
*Département de Physique, Université de Montréal, Montréal, Québec, Canada*
*Luc.stafford@umontreal.ca

Radial and axial profiles of the average electron energy along atmospheric-pressure argon plasma columns sustained by electromagnetic surface waves in the microwave regime were determined using optical emission spectroscopy (OES) coupled with a collisional radiative model. Studies were also extended to Ar/hexamethyldisiloxane (HMDSO) and Ar/HMDSO/$O_2$ plasma columns and plasma jets relevant to the growth of organosilicon nanomaterials (SiOCH and SiOx).

## 1. Introduction

In recent years, there has been a strong interest in the development of atmospheric-pressure plasma sources for the growth of functional coatings and nanomaterials on various substrates. However, for many applications, several scientific and technological challenges must be addressed before these plasma-based processes can be successfully implemented on industrial lines [1]. Among those, spatial inhomogeneties of the plasma characteristics as a result of filamentation, contraction and self-organization are crucial for uniform treatments over large area substrates [1]. When operated in presence of reactive precursors for plasma enhanced chemical vapour deposition (PECVD) of nanostructured thin films, gas-phase kinetics can also become highly complex, with the increasing relative contribution of 3-body collisions. For such PECVD applications, a crucial aspect to control is the precursor dissociation dynamics yielding atoms, radicals, and ions, which can either stick to the substrate and chamber walls to produce homogeneous coatings or agglomerate by collisions in the gas-phase to form clusters and nanoparticles (nanodusty plasmas).

In this work, the results of a fundamental study on the electron kinetics and gas phase chemistry are reported for atmospheric-pressure plasmas sustained by electromagnetic surface wave in the microwave regime. First, a poly-diagnostic investigation of such plasmas operated in nominally pure Ar was performed to determine the average electron energy (or electron temperature $T_e$ assuming Maxwellian electron energy distribution function) along the microwave plasma column. This was realized by comparing the emission intensities from Ar 4p states to those predicted by a collisional-radiative model using the electron temperature and the number density of metastable Ar atoms as the only adjustable parameters. The results were then compared to $T_e$ values deduced from detailed analysis of the continuum emission as well as from the emission intensities from high-lying states (5p and above). This approach was then applied to Ar microwave plasma columns containing organosilicon precursors relevant for the growth of coatings and nanopowders. These results are used to examine the role of nanopowders formation on the electron kinetics in such complex plasmas.

## 2. Experimental arrangement and diagnostics

### 2.1 Discharge setup

The atmospheric-pressure surface wave plasma (AP-SWP) reactor is presented in Fig. 1.

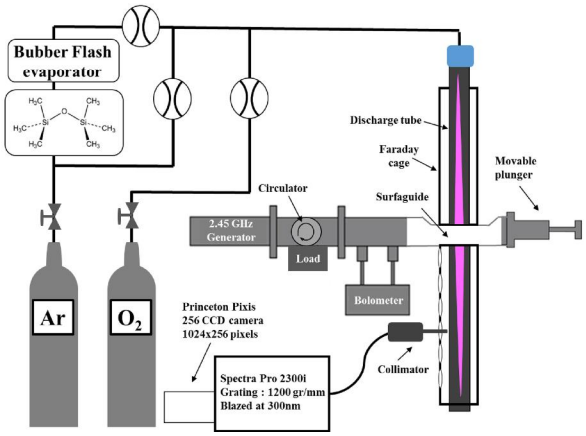


Fig. 1. Schematics of the experimental setup.

The plasma is sustained using a 2kW Sairem microwave generator operating at 2.45GHz. The microwave power is delivered and coupled to a 6 mm ID (8 mm OD) fused silica discharge tube using a surfaguide. A circulator is placed between the magnetron head and the surfaguide to direct unwanted reflections to a water-cooled load. A bidirectional coupler paired to a bolometer is used to

measure the incident and reflected powers (and thus to determine the power absorbed by the plasma). The setup is combined with a bubbler/flash evaporator to deliver specific mass flow rates of organosilicon precursors, in particular hexamethyl disiloxane (HMDSO), tetraethyl orthosilicate (TEOS), and tetramethyl cyclotetrasiloxane (TMCTS). Experiments were carried in nominally pure Ar {1SLM}, Ar/precursor {1SLM; 100 PPM} and Ar/precursor/$O_2$ {1SLM; 100 PPM; 0.001 to 0.1 SLM} gas mixtures.

### 2.2 Optical emission measurements

Plasma emission was recorded at various position along and across the microwave plasma columns using a bifurcated optical fiber connected to various spectrometers. Selected experiments were performed with a high-resolution Jobin-Yvon spectrometer (1 m focal length) for analysis of (i) the OH(A-X) emission band for determination of the rotational temperature (assumed equal to the gas temperature) and (ii) the $H_\beta$ emission line for determination of the electron density from Stark broadening. Two Avantes spectrometers were also used: the first one covers the 200 to 700 nm wavelength range with a spectral resolution (full width at half maximum) of approximately 0.4 nm while the second one covers the 700–900 nm range with a resolution of 0.2 nm. Typical emission spectra in Ar, Ar/HMDSO and Ar/HMDSO/$O_2$ plasmas are presented in Fig. 2.

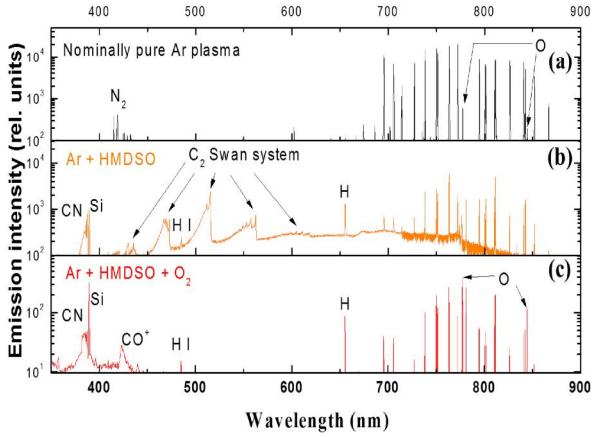


Fig. 2. OES from AP-SWP operated in (a) nominally pure Ar, (b) Ar/HMDSO and (c) Ar/HMDSO/$O_2$.

As expected the spectra from nominally pure Ar plasmas is dominated by emission from the 4p-to-4s transitions of Ar in the 700–900 nm wavelength range. Following the addition of HMDSO, many new features appear, including rovibrational bands from $C_2$ Swan molecular system and CN violet molecular system (at 388.3 nm). Si I emission lines (390.5 nm) along with H I emission lines ($H_\alpha$ at 656.2 nm and $H_\beta$ at 486.1 nm) could also be seen, suggesting very strong precursor dissociation. A broad continuum is also observed; a feature that can probably be ascribed to $C_2H$ fragments. In presence of $O_2$ in Ar/HMDSO plasmas, this continuum emission disappears. In addition, carbon fragments undergo oxidation processes, resulting in CO emission. CN emission can be attributed to the interaction between plasma-generated carbon fragments and $N_2$ due to the open-air configuration.

### 2.3 Collisional radiative model

In order to extract the electron temperature $T_e$ (assuming Maxwellian electron energy distribution function) from the Ar 4p-to-4s emission lines presented in Fig. 2, a collisional radiative (CR) model of atmospheric-pressure Ar plasmas was developed. This model assumes that the Ar 4p levels giving rise to the emission between 700 and 900 nm are excited by electron impact from either ground or 4s metastable and resonant states (see Fig. 3). It also takes into account excitation transfer processes ($Ar^*+Ar \rightarrow Ar^{**}+Ar$) among 4p manifolds by collisions with ground state Ar atoms as well as all relevant radiative decays and quenching reactions. Over the range of experimental conditions investigated, the predictions of the model were found to be fairly insensitive to the populations of Ar 4s states, indicating that stepwise excitation processes dominate over electron-impact excitation on ground state Ar atoms. As a consequence, relative emission intensities become solely dependent on the electron temperature.

At atmospheric pressure, atoms (excited as well as in ground state) and ions are significantly converted into excimer molecules ($Ar_2$) and ions ($Ar_2^+$). Therefore the associative ionization (AI) reactions ($Ar^* + Ar \rightarrow Ar_2^+ + e^-$) as well as the reverse dissociative recombination (DR) process could also influence the populations of emitting 4p levels. While DR processes represent additional creation terms in the particle balance of 4p states, AI reactions correspond to collisional losses. Thus, in the present CR model, the contribution of AI reactions was implicitly included in the quenching reaction terms. On the other hand, Sainz *et al.* [2] have shown that the DR processes mainly lead to 4s levels and therefore have negligible influence on the population of 4p levels in Ar AP-SWPs.

Based on the framework displayed in Fig. 3, the coupled steady-state particle balance equations can be solved to get the population density of Ar 4p levels using $T_e$ as the only adjustable parameter [3].

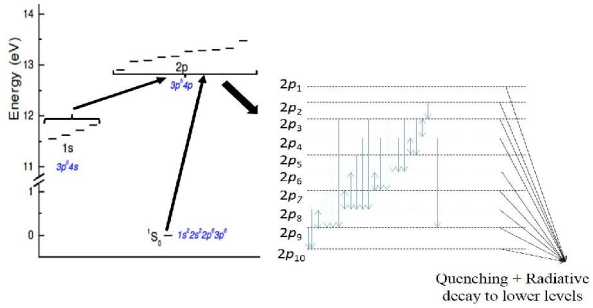


Fig. 3. CR model framework for Ar *2p* levels.

## 3. Results and discussion

### 3.1 Radial and axial profile of $T_e$ in pure Ar

The values of the electron temperature deduced from the best fit of the relative emission intensities of the 13 4p-to-4s transitions presented in Fig. 2 are shown in Fig. 4 as a function of axial position along the microwave plasma columns. Electron densities and OH rotational temperatures obtained from Stark broadening of the $H_\beta$ line and from OH(A-X) emission are also shown for comparison. $T_e$ values are in the 0.5 eV range, which is comparable to those deduced from detailed analysis of the continuum emission (assuming a dominant contribution from electron-atom Bremsstrahlung [4]) as well as from the emission intensities from high-lying Ar states (5p and above for which Boltzmann equilibrium is valid)[5].

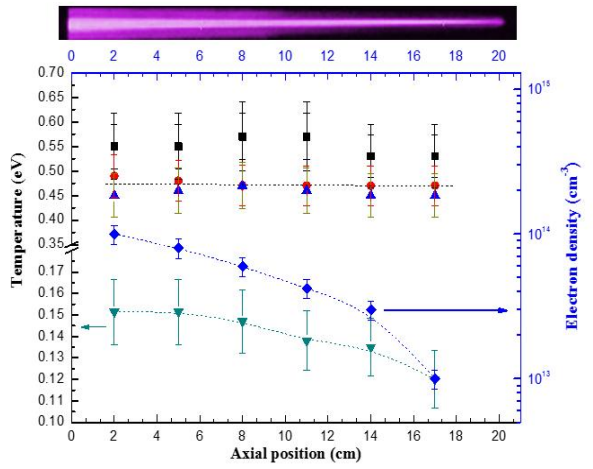


Fig. 4. Axial profile of: ■ $T_{exc}$ using Boltzmann diagram of Ar-I lines originating from high lying levels (>5p); ● $T_e$ using CR model and 4p-to-4s Ar-I lines; ▲ $T_e$ using continuum emission; ▼ $T_{rot}$ (=$T_g$); ♦ $n_e$.

Despite the significant change in $n_e$ and $T_g$ along the microwave plasma column due to the non-axially uniform power deposition of the electromagnetic surface wave, a constant value of $T_e$ is observed [6]. This experimental result is in good agreement with the predictions of a self-consistent 2D fluid model coupled with the resolution of Maxwell's equations for the surface-wave [7].

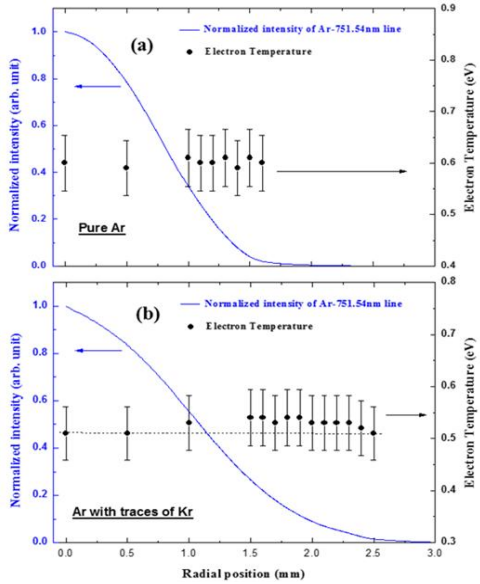


Fig. 5. Radial profile of $T_e$ in a (a) contacted plasma (pure Ar) (b) diffuse plasma (Ar with 1% Kr).

Fig. 5(a) presents the radial profile of the Ar 751.5 nm emission intensity (in relative units) obtained after Abel inversion in a nominally pure Ar (contracted) plasma. As a result of contraction, emission intensity is non-zero only up to about 1.5 mm from the axis. Despite contraction, $T_e$ is constant along the discharge radius. Similar findings were obtained following the addition of 1% Kr in Ar leading to a more diffuse plasma column (a feature that can be attributed to the quenching of Ar metastable atoms by collisions with Kr atoms, producing significant amount of $Kr^+$ ions instead of the $Ar_2^+$ ions otherwise produced through metastable associative-ionization reactions). Despite the non-homogeneities of the electric field in surface-wave plasma columns [7], the radially-homogeneous $T_e$ values presented in Fig. 5 can be attributed to the non-local power deposition dynamics in such plasmas, even under atmospheric-pressure conditions. Indeed, calculations of the energy relaxation length for $T_e$=0.5 eV reveals $\lambda_\varepsilon$=1.1 mm, which is comparable to the diffusion length $\Lambda = R/2.405 = 1.25$ mm (recall that the local approximation requires $\lambda_\varepsilon << \Lambda$).

### 3.2 $T_e$ in Ar/HMDSO & Ar/HMDSO/$O_2$ plasmas

In presence of HMDSO in the nominally pure microwave Ar plasma, nano-powders start to form on the discharge tube walls (see TEM images displayed in Fig. 6). While Ar/HMDSO plasmas produced highly inhomogeneous nanostructures with tube and sheet like nano-features, Ar/HMDSO/$O_2$ plasmas yields to round-like nanoparticles with an average size of 50 nm.

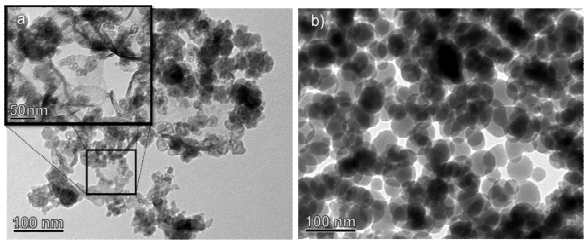


Fig. 6. TEM images from powders obtained in (a) Ar/HMDSO, (b) Ar/HMDSO/$O_2$ plasmas.

FTIR analysis of the nano-powders are presented in Fig. 7. With no $O_2$ injected in the gas phase, the FTIR spectrum displays $Si(CH_3)_2$ and $Si(CH_3)_3$ peaks around 800 $cm^{-1}$ as well as $CH_x$ peaks between 2878 $cm^{-1}$ and 2900 $cm^{-1}$; this result is consistent with the formation of SiOCH. As $O_2$ is introduced in the Ar/HMDSO plasma, all organosilicon peaks decrease while the Si-O-Si bands (for example those due to rocking mode around 450 $cm^{-1}$ and vibrational mode at 1070 $cm^{-1}$) increase. A similar increase is observed for the broad OH band around 3340 $cm^{-1}$ attributed to OH vibration in (Si or C)-OH groups. At higher $O_2$ concentrations, most organic compounds have been removed due to the formation of volatile compounds (for example, $CH_2O$, $CH_2O_2$, CO, $CO_2$), such that the powders can be attributed to silicon oxide with almost no traces of carbon.

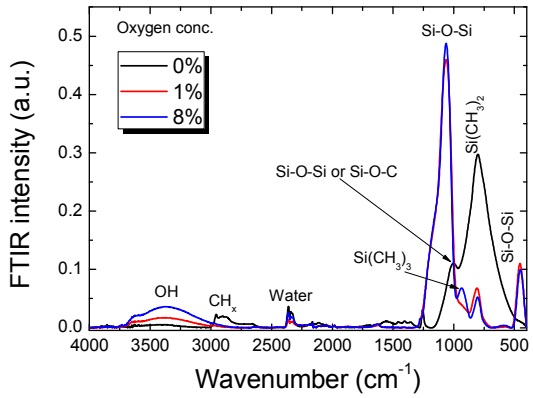


Fig. 6. Influence of addition of $O_2$ in Ar/HMDSO plasma on the FTIR spectrum from the nano-powders.

The electron temperature in Ar/HMDSO and Ar/HMDSO/$O_2$ plasmas determined using the approach described above is presented in Fig. 8. $T_e$ values first increase with the addition of 100 ppm of HMDSO (region 1 in Fig. 8); this result is consistent with the formation of SiOCH and the expected attachment of electrons on these nano-powders. Following the addition of $O_2$ in the Ar/HMDSO plasma, $T_e$ decreases (region 2 in Fig. 8). Based on the FTIR analysis and the OES spectra displayed in Figs. 2 and 6, this result must be linked to the formation of volatile carbon-oxide groups. $T_e$ values then again increase with the addition of $O_2$ up to a plateau when essentially $SiO_x$ nano-powders are formed (region 3 in Fig. 8). The higher electron temperatures when $SiO_x$ nano-powders are formed in $O_2$-rich Ar/HMDSO/$O_2$ plasmas with respect to the values when SiOCH nano-powders are formed in Ar/HMDSO plasmas suggests different electron attachment dynamics on "metallic" versus "dielectric" nano-powders.

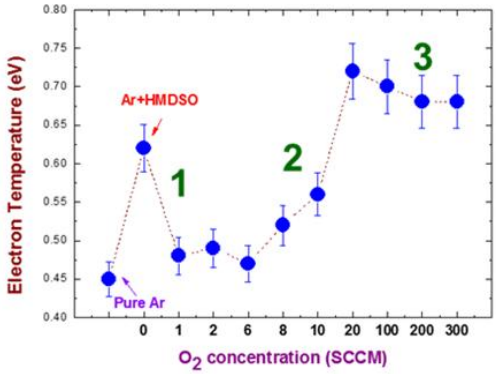


Fig. 8. Influence of $O_2$ addition in Ar/HMDSO plasmas on the electron temperature determined from Ar 4p-to-4s emission lines and CR model.

### 4. Acknowledgments

The authors would like to acknowledge the financial support from the National Sciences and Engineering Research Council of Canada (NSERC), the Fonds de Recherche du Québec – Nature et Technologies (FRQNT) and Plasmionique.

### 5. References

[1] A. Kilicaslan, *et al*, *J. Appl. Phys*., **115**, 113301 (2014).
[2] A. Sainz *et al*, *J. Appl. Phys*., **97**, 113305 (2005).
[3] R. K. Gangwar *et al*, (in preparation).
[4] E. Iordanova *et al*, J. *Phys. D. Appl. Phys*. **41**, 015208 (2008).
[5] M.D. Calzada *et al*, *J. Appl. Phys.* **80**, 46 (1996).
[6] M. A. Ridenti, *et al*, *J. Phys. D*, **20**, 197 (2014).
[7] Y. Kabouzi *et al*, *Phys. Rev. E,* **75**, 016402 (2007).